

Dynamic Domains, Dynamic Solutions: DPCore for Continual Test-Time Adaptation

Yunbei Zhang¹, Akshay Mehra¹, Jihun Hamm¹

¹Tulane University

{yzhang111, amehra, jhamm3}@tulane.edu

Abstract

Continual Test-Time Adaptation (CTTA) seeks to adapt a source pre-trained model to continually changing, unlabeled target domains. Existing TTA methods are typically designed for environments where domain changes occur sequentially and can struggle in more dynamic scenarios, as illustrated in Figure 1. Inspired by the principles of online K-Means, we introduce a novel approach to CTTA through visual prompting. We propose a *Dynamic Prompt Coreset* that not only preserves knowledge from previously visited domains but also accommodates learning from new potential domains. This is complemented by a distance-based *Weight Updating Mechanism* that ensures the coreset remains current and relevant. Our approach employs a fixed model architecture alongside the coreset and an innovative updating system to effectively mitigate challenges such as catastrophic forgetting and error accumulation. Extensive testing on four widely-used benchmarks demonstrates that our method consistently outperforms state-of-the-art alternatives in both classification and segmentation CTTA tasks across the structured and dynamic CTTA settings, with 99% fewer trainable parameters.

Introduction

Deep Neural Networks (DNNs) have achieved remarkable success due to their ability to model complex patterns and relationships within data. However, their performance is often significantly compromised when there is a domain discrepancy between the training data and the test environment. This misalignment can lead to substantial degradation in model accuracy and reliability, a challenge commonly encountered in real-world applications (Recht et al. 2019; Hendrycks and Dietterich 2019; Koh et al. 2021).

To mitigate this issue, Test-Time Adaptation (TTA) (Sun et al. 2020; Liang, He, and Tan 2023; Liang, Hu, and Feng 2020) has emerged as an effective strategy. TTA aims to adjust pre-trained models to new domains during test time without the need for extensive retraining or labeled data. Its minimal overhead compared to other adaptation strategies makes TTA particularly well-suited for real-world applications. Traditional TTA methods, such as Tent (Wang et al. 2021) are tailored for scenarios involving a stationary single target domain. While effective, these approaches assume a static or singular shift in the data distribution, which may not adequately capture the complexities of real-world environments. Aiming to address continually changing target

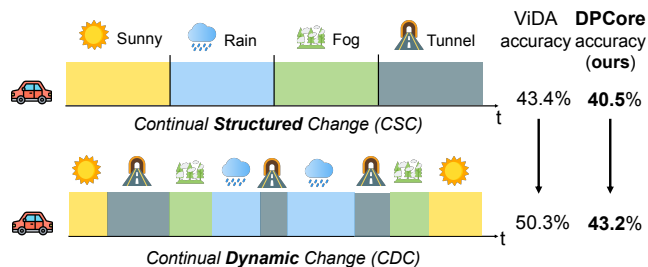


Figure 1: The top panel illustrates the *Continual Structured Change (CSC)* setting with predictable domain transitions, while the bottom panel shows the *Continual Dynamic Change (CDC)* setting, featuring rapid and unpredictable domain shifts. Performance (error rate \downarrow) on ImageNet-to-ImageNet-C demonstrates that our DPCore method outperforms ViDA in both settings, particularly excelling in the more challenging CDC scenario.

domains, Continual Test-Time Adaptation (CTTA) (Wang et al. 2022; Niu et al. 2022) methods like CoTTA (Wang et al. 2022) have been developed. However, these methods typically assume that domain shifts occur in a structured and predictable sequence (*Continual Structured Change (CSC)* in Fig. 1), an assumption that rarely aligns with practical scenarios where domain shifts can be unstructured and dynamic (*Continual Dynamic Change (CDC)* in Fig. 1), varying in domain duration and timing of changes.

The *CDC* setting introduced in our study distinctly diverges from the conventional *CSC* setting in two significant ways: First, in the *CDC* setting, a domain can recur multiple times within a given time interval, as opposed to the *CSC* setting where each domain appears only once (e.g., ImageNet-to-ImageNet-C task). Second, while *CSC* typically maintains uniform domain lengths, *CDC* features varying domain durations—from very brief to extended periods. For example, consider a vision model used in an autonomous driving vehicle, tasked with recognizing road conditions and objects such as vehicles and pedestrians. In a *CSC* setting, a vehicle transitioning sequentially from sunny to rainy to dark tunnel conditions might adapt more straightforwardly. Conversely, the *CDC* setting represents a more dynamic and challenging environment. Here, a vehicle might frequently and unpredictably navigate through changing conditions—entering and exiting dark tunnels, encountering fog,

or cycling back to sunny conditions. These rapid and unpredictable domain shifts, such as transitioning from sunny to dark to fog to rain and back, present substantial adaptation challenges that are more reflective of real-world dynamics. Moreover, ViDA (Liu et al. 2023b), a SOTA CTTA method, demonstrates the challenge of dynamic domains with its performance dropping significantly—from an error rate of 43.4% to 50.3% on ImageNet-C—when transitioning from *CSC* to *CDC*, as depicted in Fig. 1.

To this end, we introduce a novel method **DPCore** for CTTA. It enhances pre-trained model performance in dynamically changing environments while addressing catastrophic forgetting and error accumulation. DPCore employs a pseudo-label-free strategy, relying on direct distributional alignment to learn visual prompts without altering the source model. As shown in Fig 2, central to DPCore is a *Dynamic Prompt Coreset*, adaptively updated to preserve knowledge from previously encountered domains and seamlessly integrate insights from new, potentially unseen domains. This dynamic coreset acts as a living memory of the model’s experiences, enabling it to maintain historical context and continuity across shifts in the data landscape. Additionally, DPCore features a sophisticated *Weighted Updating Mechanism* that adjusts prompts based on the calculated distance between the statistics of the current batch and those aggregated in the coreset. Leveraging these distance-based weights, DPCore dynamically tailors the adaptation process to the specific characteristics of incoming data, enhancing the model’s responsiveness to new patterns.

We benchmarked our method, DPCore, against leading baselines including ViDA (Liu et al. 2023b), SAR (Niu et al. 2023), VDP (Gan et al. 2023), and EcoTTA (Song et al. 2023) across four widely-used CTTA benchmarks in both conventional *CSC* and our innovative *CDC* settings. DPCore significantly outperformed the competition on ImageNet-to-ImageNet-C with a **15.3% accuracy improvement** over the source pre-trained model, exceeding ViDA by a margin of **2.9%**. Additionally, our method demonstrated robust enhancements in the more challenging *CDC* setting, where prior CTTA approaches often struggle. Our performance, measured at 56.8%, significantly surpasses ViDA’s 49.7%, showing a **notable accuracy improvement of 7.1%** in this setting. Beyond classification, DPCore also surpasses previous SOTA methods in semantic segmentation tasks by mIoU scores of **0.9%** in the *CSC* setting and **1.8%** in the *CDC* setting, all while utilizing **99% fewer parameters** required by ViDA. Furthermore, our method maintains computational and memory efficiency, making it a practical solution for real-world applications. Our contribution can be summarized as follows:

- We introduce DPCore, which utilizes a *dynamic prompt coreset* and a *weighted updating mechanism* to store and update the model’s experiences, effectively addressing fundamental challenges in continual learning such as catastrophic forgetting and error accumulation.
- We propose a more realistic and challenging CTTA setting, *Continual Dynamic Change (CDC)*, where domains change rapidly and unpredictably with variations in do-

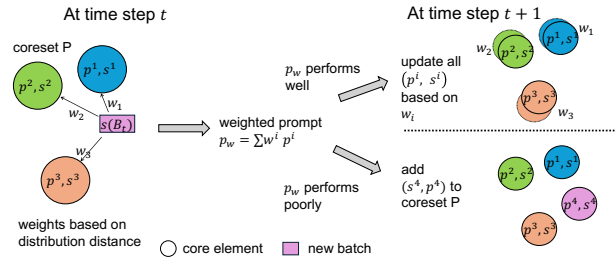


Figure 2: An overview of DPCore. When the batch B_t arrives, its weights w and prompts p_w can be computed quickly. If p_w reduces the domain shift, e.g., when B_t is similar to a previously seen domain (called ID), the corresponding core elements are updated. If p_w performs poorly, e.g., when B_t is from an unseen domain (called OOD), a new core element is added to the coreset.

main duration and timing of changes, presenting difficulties that prior CTTA methods struggle to overcome.

- We validate the efficacy and efficiency of DPCore against SOTA for classification and segmentation tasks across the *CSC* and *CDC* settings. Furthermore, we provide an analytical explanation of DPCore’s robustness against domain shifts, demonstrating its superior adaptability.

Related Work

Test-Time Adaptation (TTA) (Liang, He, and Tan 2023; Sun et al. 2020; Wang et al. 2021) aims to improve the performance of pre-trained models with unlabeled data when deployed in unseen domains. Traditional TTA methods (Wang et al. 2021; Iwasawa and Matsuo 2021; Liang, Hu, and Feng 2020; Gao et al. 2023; Schneider et al. 2020; Mirza et al. 2022, 2023; Niu et al. 2024), such as Tent (Wang et al. 2021), which updates batch normalization parameters by minimizing entropy, and SAR (Niu et al. 2023), which investigates the robustness of normalization layers, typically focus on adapting to a single, stationary target domain. While these methods are effective in static settings, they frequently struggle to maintain performance in environments where the target domain undergoes continual changes.

Continual Test-Time Adaptation (CTTA) (Wang et al. 2022; Lee, Yoon, and Hwang 2024; Niu et al. 2022; Niloy et al. 2024; Liu et al. 2023a; Boudiaf et al. 2022; Gong et al. 2022; Yuan, Xie, and Li 2023) assumes that target domains are not stationary but change continuously. This challenging task is first introduced in (Wang et al. 2022), which proposed a teacher-student framework for generating pseudo-labels from the teacher model. EcoTTA (Song et al. 2023) introduces a meta-network and self-distilled regularization. (Gan et al. 2023; Gao et al. 2022; Liu et al. 2023b) utilize visual prompts or adapters to capture the domain-invariant and domain-specific features. While these approaches demonstrate effectiveness in the *CSC*, they tend to struggle in the *CDC* setting, a more challenging environment that demands higher adaptability (as illustrated in Fig. 1). Our method is specifically designed to improve the performance of the source pre-trained model across both *CSC* and *CDC* settings.

Method

Problem Definition

We are given a pre-trained model $f_\theta(x)$ with parameters θ on the labeled source data $\mathcal{D}^s = \{(\mathbf{x}_i^s, y_i^s)\}_{i=1}^{N^s}$. The dataset \mathcal{D}^s comprises i.i.d. samples from a probability distribution $P^s(X, Y)$. The model f is a composition $f = h \circ \phi$ of the feature extractor $\phi : \mathcal{X} \rightarrow \mathcal{Z}$ and the classifier $h : \mathcal{Z} \rightarrow \mathcal{Y}$. During testing, the model f will be evaluated on unlabeled target samples from an unknown number M of target domains $\mathcal{D}^1, \dots, \mathcal{D}^M$. In the online setting, the model f encounters a sequence of test data batch B_1, B_2, \dots, B_t where t can go to infinity. We operate under the assumption that all examples in a single batch is from the same (unknown) domain, but each batch may be from different domains. In general, TTA aims to adapt the model to each incoming test batch B_t at time step t and update its parameters from $\theta_t \rightarrow \theta_{t+1}$ in order to improve its prediction on the subsequent batch B_{t+1} .

Visual Prompting

In this paper, we mainly focus on Vision Transformers (ViTs) (Dosovitskiy et al. 2021; Liu et al. 2021). Denote the patch embeddings of an input image x as $\{\mathbf{E}_i\}_{i=1}^k$. The inputs to the transformer layers consist of these encoded patch tokens augmented with a special classification token [CLS]. The prediction of the vision transformer can be formulated as $[\text{CLS}] = \phi([\text{CLS}], \{\mathbf{E}_i\}_{i=1}^k)$ and $\hat{y} = h([\text{CLS}])$, where $[\cdot]$ represents concatenation of tokens. Incorporating a visual prompt into the ViT represents a parameter-efficient approach for fine-tuning or adapting the model, particularly when the model is fixed (Jia et al. 2022; Ge et al. 2023). By introducing l prompt tokens $\mathbf{p} := \{[\text{Prompt}]_i\}_{i=1}^l$, the prediction process can be reformulated as follows:

$$\begin{aligned} [\text{CLS}] &= \phi([\mathbf{p}], [\text{CLS}], \{\mathbf{E}_i\}_{i=1}^k) \\ \hat{y} &= h([\text{CLS}]) \end{aligned} \quad (1)$$

In the context of TTA, prompts can be optimized using consistency maximization, entropy minimization, or unsupervised distribution alignment (Niu et al. 2024; Sun et al. 2023; Gao et al. 2022). In this work, we focus on marginal distribution alignment (Ben-David et al. 2006; Le et al. 2021; Shen et al. 2018) to bypass the reliance on pseudo labels, which often contribute to error accumulation in continual learning scenarios. Specifically, for the online setting, at time step t , the prompts from last time step \mathbf{p}_{t-1} can be adaptively learned on the batch B_t by

$$\mathbf{p}_t = \arg \min_{\mathbf{p}} d(\phi(\mathcal{D}^s), \phi(B_t; \mathbf{p}_{t-1})) \quad (2)$$

where d is a distribution distance and \mathbf{p}_0 is a random initialized prompts. Considering the limited amount of data in each test time batch, we match the statistics of the target batch $\mathbf{s}(B_t; \mathbf{p}_{t-1})$ and of the source \mathbf{s}^s :

$$\begin{aligned} d(\mathbf{s}^s, \mathbf{s}(B_t; \mathbf{p}_{t-1})) &= \|\boldsymbol{\mu}^s - \boldsymbol{\mu}(B_t; \mathbf{p}_{t-1})\|_2 + \\ &\quad \|\boldsymbol{\sigma}^s - \boldsymbol{\sigma}(B_t; \mathbf{p}_{t-1})\|_2 \\ \text{where } \mathbf{s}^s &:= (\boldsymbol{\mu}^s, \boldsymbol{\sigma}^s) = (\boldsymbol{\mu}(\phi(\mathcal{D}^s)), \boldsymbol{\sigma}(\phi(\mathcal{D}^s))), \\ \mathbf{s}(B_t; \mathbf{p}_{t-1}) &:= (\boldsymbol{\mu}(B_t; \mathbf{p}_{t-1}), \boldsymbol{\sigma}(B_t; \mathbf{p}_{t-1})) \\ &= (\boldsymbol{\mu}(\phi(B_t; \mathbf{p}_{t-1})), \boldsymbol{\sigma}(\phi(B_t; \mathbf{p}_{t-1}))) \end{aligned} \quad (3)$$

Here the statistics are calculated in the representation space. Our method necessitates only the basic statistical parameters—mean $\boldsymbol{\mu}^s$ and variance $\boldsymbol{\sigma}^s$ —from the source data.

Dynamic Prompt Coreset (DPCore)

In this work, we introduce DPCore, shown in Fig. 2 with three key components: Visual Prompting, *Dynamic Prompt Coreset*, and *Weighted Updating Mechanism*.

Dynamic Prompt Coreset. For anti-forgetting continual test-time adaptation in continually changing environments, we introduce a dynamic prompt coreset, inspired by Online K-Means (Duda and Hart 1973), to preserve the knowledge learned on visited domains. This coreset, denoted as P , is initialized as empty and is adaptively updated at each time step t . The update occurs in two distinct ways: 1) If the current batch B_t represents a potentially new domain not covered by the coreset, prompts \mathbf{p}_t are learned from scratch for a larger number of steps (E_{OOD}). This approach prevents error accumulation and integrates the newly learned prompt alongside batch statistics $(\mathbf{p}_t, \mathbf{s}(B_t))$, termed a core element, into P for future reference. 2) If B_t is assessed to be from a domain already represented within the coreset, then the coreset updates all existing core elements according to specific weights discussed later. This dynamic adjustment ensures the coreset remains relevant and reflective of the evolving data distribution, thus preserving knowledge across visited domains efficiently. Moreover, it prevents the model from inappropriately applying outdated knowledge from significantly different domains to new situations, thereby reducing error accumulation.

Weighted Updating Mechanism. We define the distance between the target batch B_t with the prompt \mathbf{p}_{t-1} as

$$d(B_t; \mathbf{p}_{t-1}) := d(\mathbf{s}^s, \mathbf{s}(B_t; \mathbf{p}_{t-1})) \quad (4)$$

and distance without any prompt *i.e.* the frozen source pre-trained model as:

$$d(B_t) := d(\mathbf{s}^s, \mathbf{s}(B_t)) \quad (5)$$

The weights are computed based on the distance between the target batch and source statistics. At time step t , suppose there are k core elements $\{(\mathbf{p}^1, \mathbf{s}^1), \dots, (\mathbf{p}^k, \mathbf{s}^k)\}$ in the coreset P . We first compute the statistics $\mathbf{s}(B_t)$ without any prompts and generate weighted prompts based on the distance between $\mathbf{s}(B_t)$ and all statistics in the P :

$$\begin{aligned} \mathbf{p}_w &:= \sum_{i=1}^k w^i \mathbf{p}^i \\ \text{where } w^i &= \frac{\exp(-d(\mathbf{s}(B_t), \mathbf{s}^i)/\tau)}{\sum_{j=1}^k \exp(-d(\mathbf{s}(B_t), \mathbf{s}^j)/\tau)}. \end{aligned} \quad (6)$$

τ is the temperature factor.

The new batch is then processed by the pre-trained model with the weighted prompts \mathbf{p}_w to determine if this new batch is coming from a potential new domain. If the batch is from a previously encountered domain, the corresponding prompts in the coreset will have larger weights, aiding in reducing the gap between the new batch and the source distribution. We assess this by comparing the distance with weighted prompts $d(B_t; \mathbf{p}_w)$ against $d(B_t)$. A significant decrease in this distance indicates the batch is similar to previously seen domains, and therefore we update the weighted prompts for

a smaller number of steps E_{ID} to refine p_t . The coreset’s prompts and statistics are adaptively updated based on their weights w^i and an updating weight α :

$$p^i \leftarrow p^i + \alpha w^i (p_t - p^i), \quad s^i \leftarrow s^i + \alpha w^i (s_t - s^i) \quad (7)$$

where $s = (\mu, \sigma)$. Note that $\max\{0, (\sigma^t - \sigma^i)\}$ is used in the update to prevent negative σ . A predefined threshold ratio ρ helps formally identify whether a batch is from a new domain. The model processes the batch with p_t and subsequently returns the prediction.

The strength of the algorithm is twofold. First, the algorithm learns the prompts not merely from a single batch but potentially from the homogeneous domain group, allowing for more comprehensive adaptation. Second, error accumulation is mitigated because the prompt for one domain is generally not updated when faced with a significantly different domain. The algorithm is presented in Alg. 1.

Analysis

In this section, we provide an intuition on why our method is robust to dynamic domain changes, unlike other TTA methods. Our algorithm is inspired by the online/sequential K-Means algorithm (see Sec. 10.11 of (Duda and Hart 1973)). We will therefore consider a simplified version of Alg. 1 (Appendix) where instead of a general weight w we consider a one-hot weight, that is, only the closest core element of a given test batch is considered. Suppose the batches B_0, \dots, B_t are naturally clustered into M mutually exclusive clusters G_1, \dots, G_M based on their distances.

Let $\Pi^{(t-1)}$ be the set of permutations on $(1, \dots, t-1)$, $G_i(t)$ be the set of batches in i -th cluster at time t , and $s^i(t)$ be the i -th core element (or center) at time t . We assume the clusters are *well-separated* (see Appendix for definition and for full proofs).

Proposition 1. *For any $t \geq 1$, Alg. 2 assigns correct clusters to all the batches B_1, \dots, B_t .*

Proposition 2. *For any $t > 1$, Alg. 2 assigns B_t to the correct cluster independent of the batch order $B_{\pi(1)}, \dots, B_{\pi(t-1)}$, $\forall \pi \in \Pi^{(t-1)}$. Furthermore, if $\alpha = \frac{1}{|G_j|}$, then the core element $s^i(t)$ is the group mean $s^i(t) = \frac{1}{|G_i(t)|} \sum_{B \in G_i(t)} B$ which is also independent of the order of B_1, \dots, B_t .*

Proposition 3. *For any $t > 1$, Alg. 2 returns the prompt p_t for batch B_t independent of the batch order $B_{\pi(1)}, \dots, B_{\pi(t-1)}$, $\forall \pi \in \Pi^{(t-1)}$.*

Remarks Under the simple model and the well-separatedness assumption, we showed why the coreset-based approach is provably robust to random domain changes. This analysis is to serve as an intuition, and the full proof of the robustness of Alg. 1 under general conditions is left for future work.

Experiments

Experimental Setup

Datasets. We evaluate our proposed method on three classification datasets: ImageNet-ImageNet-C, CIFAR100-CIFAR100C, and CIFAR10-CIFAR10C (Hendrycks and

Algorithm 1: The proposed algorithm DPCore

Input: A source pre-trained model $f(x)$, source statistics s^s , test batches $\{B_t\}_{t=1}^T$

Initialization: An empty coreset, and random prompt tokens.

```

1: for the first batch  $B_1$  do
2:   Compute the statistics of batch  $B_1$  without prompt.
3:   Learn prompt from scratch (Eq. 2).
4:   Add the batch statistics and prompt to the empty coreset.
5: end for
6: for  $t = 2, \dots, T$  do
7:   Compute the statistics of batch  $B_t$  without prompt.
8:   Compute the weights and weighted prompts (Eq. 6).
9:   Compute batch statistics with the weighted prompt.
10:  Compare distances with/w.o. weighted prompt (Eq. 4/5).
11:  if  $B_t$  is ID samples then
12:    Update weighted prompt on  $B_t$  by 1 step.
13:    Update all coreset elements (Eq. 7).
14:  else
15:    Learn prompt from scratch (Eq. 2).
16:    Add the batch statistics and learned prompt to the coreset as a new element.
17:  end if
18: end for

```

Output: Prediction for all batches; The learned coreset.

Dietterich 2019). Each dataset comprises corrupted images in 15 types of corruption, categorized into four main groups. Our experiments use the highest level of corruption (i.e. severity 5). Furthermore, we also validate DPCore on a CTTA segmentation task: Cityscapes-ACDC (Sakaridis, Dai, and Gool 2021; Cordts et al. 2016).

CSC and CDC Settings. We evaluate DPCore across the CSC and CDC settings. The CSC setting follows the implementation by (Wang et al. 2022). In the CDC setting, we dynamically generate the order of domain batches to closely simulate real-world variability. This process begins with randomly selecting a domain from the available pool. We then randomly determine the number of batches to be sampled from this domain, ensuring that both the duration of each domain and the timing of domain changes are unpredictable. Uniform distribution is used in our reported results. Other distributions are discussed in the Appendix.

Implementation Details. To ensure consistency and comparability in our experiments, we follow the implementation details specified in CoTTA (Wang et al. 2022) and ViDA (Liu et al. 2023b). For classification tasks, we use the ViT-Base model pre-trained on the ImageNet 1K dataset (Wightman 2019), further fine-tuning it on clean CIFAR10/100 training sets for CIFAR10/100C tasks. For segmentation, we employ the pre-trained Segformer-B5 model (Xie et al. 2021). We utilize the AdamW optimizer (Loshchilov and Hutter 2017; Kingma and Ba 2014) with a 0.1 learning rate.

Methods Compared. We compare our method against strong CTTA baselines including Tent (Wang et al. 2021), SAR (Niu et al. 2023), CoTTA (Wang et al. 2022), VDP (Gan et al. 2023), DePT (Gao et al. 2022), EcoTTA (Song et al. 2023), and ViDA (Liu et al. 2023b). More details can be found in the Appendix.

Fairness with Other Methods. The reported results for

Table 1: **Classification error rate (%) for ImageNet-to-ImageNet-C in the *Continual Structured Change (CSC)* setting.** Our method outperforms the second-best by **2.9%** in this conventional CTTA setting.

Algorithm	Gauss.	Shot	Impulse	Defocus	Glass	Motion	Zoom	Snow	Frost	Fog	Bright	Contrast	Elastic	Pixel	JPEG	Mean↓	Gain↑
Source	53.0	51.8	52.1	68.5	78.8	58.5	63.3	49.9	54.2	57.7	26.4	91.4	57.5	38.0	36.2	55.8	0.0
Pseudo (Lee 2013)	45.2	40.4	41.6	51.3	53.9	45.6	47.7	40.4	45.7	93.8	98.5	99.9	99.9	98.9	99.6	61.2	-5.4
Tent (Wang et al. 2022)	52.2	48.9	49.2	65.8	73.0	54.5	58.4	44.0	47.7	50.3	23.9	72.8	55.7	34.4	33.9	51.0	+4.8
CoTTA (Wang et al. 2022)	52.9	51.6	51.4	68.3	78.1	57.1	62.0	48.2	52.7	55.3	25.9	90.0	56.4	36.4	35.2	54.8	+1.0
VDP (Gan et al. 2023)	52.7	51.6	50.1	58.1	70.2	56.1	58.1	42.1	46.1	45.8	23.6	70.4	54.9	34.5	36.1	50.0	+5.8
SAR (Niu et al. 2023)	45.8	45.9	47.7	52.3	63.7	46.2	50.9	40.3	42.4	41.8	24.4	53.4	53.6	38.4	36.6	45.6	+10.2
EcoTTA (Song et al. 2023)	48.1	45.6	46.3	56.5	67.1	50.4	57.1	41.3	44.5	43.8	24.1	71.6	54.8	34.1	34.8	48.0	+7.8
ViDA (Liu et al. 2023b)	47.7	42.5	42.9	52.2	56.9	45.5	48.9	38.9	42.7	40.7	24.3	52.8	49.1	33.5	33.1	43.4	+12.4
DPCore (Proposed)	42.0	38.4	40.2	46.6	55.2	44.6	46.8	37.2	38.7	39.1	22.1	50.4	45.7	30.5	30.5	40.5	+15.3

Table 2: **Classification error rate (%) for ImageNet-to-ImageNet-C in the *Continual Dynamic Change (CDC)* setting.** We introduce a novel scenario in which the target domains change dynamically, challenging prior CTTA approaches. Our method consistently outperforms ViDA by a substantial margin of **7.1%**.

Algorithm	Gauss.	Shot	Impulse	Defocus	Glass	Motion	Zoom	Snow	Frost	Fog	Bright	Contrast	Elastic	Pixel	JPEG	Mean↓	Gain↑
Source	53.0	51.8	52.1	68.5	78.8	58.5	63.3	49.9	54.2	57.7	26.4	91.4	57.5	38.0	36.2	55.8	0.0
Tent (Wang et al. 2022)	54.1	53.2	52.9	66.7	74.6	56.6	61.2	49.2	52.3	57.5	32.1	90.4	56.1	37.7	37.1	55.4	+0.4
CoTTA (Wang et al. 2022)	52.4	52.2	51.1	68.4	76.3	57.9	62.1	48.7	53.1	55.1	26.1	88.9	57.1	37.6	38.2	55.0	+0.8
VDP (Gan et al. 2023)	53.5	52.6	51.5	58.1	73.1	53.4	60.1	42.1	45.3	58.2	25.1	82.2	56.6	35.7	36.3	52.3	+3.5
SAR (Niu et al. 2023)	47.0	46.1	46.1	56.1	66.4	49.9	55.1	41.1	44.8	50.9	23.6	65.3	54.2	32.9	31.4	47.4	+8.1
EcoTTA (Song et al. 2023)	48.9	46.5	47.5	59.2	71.2	54.1	59.8	41.4	43.9	57.2	24.0	84.1	55.2	33.4	35.3	50.8	+5.0
ViDA (Liu et al. 2023b)	47.8	47.2	46.6	57.7	71.6	52.7	59.6	40.1	39.4	60.5	24.1	83.9	57.9	33.6	31.4	50.3	+5.5
DPCore (Proposed)	42.7	40.4	42.2	57.4	61.0	51.1	52.4	35.8	41.0	38.8	22.1	55.4	48.3	31.1	28.1	43.2	+12.6

Table 3: **Average error rate (%) for CIFAR10-to-CIFAR10C and CIFAR100-to-CIFAR100C across CSC and CDC settings.** Full results are in the Appendix.

Setting	Task	Metric	Source	Tent	CoTTA	VDP	ViDA	DPCore
CSC	CIFAR10C	Mean↓	28.2	23.5	24.6	24.1	20.7	18.4
		Gain↑	0.0	+4.7	+3.6	+4.1	+7.5	+9.8
	Cifar100C	Mean↓	35.4	32.1	34.8	35.0	27.3	25.1
		Gain↑	0.0	+3.3	+0.7	+0.4	+8.1	+10.3
CDC	CIFAR10C	Mean↓	28.2	26.2	27.1	25.0	23.6	20.2
		Gain↑	0.0	+2.0	+1.1	+3.2	+4.6	+8.0
	Cifar100C	Mean↓	35.4	33.5	35.9	36.1	29.8	27.4
		Gain↑	0.0	+1.9	-0.5	-0.7	+5.6	+8.0

methods like VDP, EcoTTA, and ViDA rely on using source data to initialize trainable parameters. For example, VDP (Gan et al. 2023) requires training the source model on the source domain (e.g., ImageNet) for three epochs to initialize visual domain prompts, a process that can be quite time-consuming. In contrast, our method requires only source statistics, an advantage when source data privacy is paramount and when reducing preparation time is crucial. Moreover, unlike EcoTTA (Song et al. 2023), which demands labeled source data for initialization, our method does not require any source domain labels. Our prompt token initialization is random, eliminating the need for any preliminary warm-up.

Evaluation in the CSC Setting

ImageNet-to-ImageNet-C. We initially tested our method in the conventional CSC setting, where the fifteen types of corruption occur sequentially during test time. As shown in Table 1, DPCore significantly outperformed all existing methods, achieving a **15.3%** improvement over the source pre-trained model and a **2.9%** improvement over the previous SOTA. Notably, DPCore excelled across all 15 types

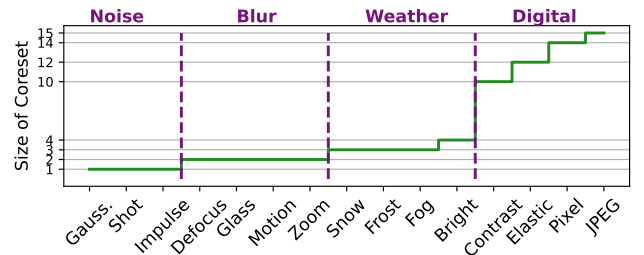


Figure 3: **Growth of coreset for ImageNet-to-ImageNet-C in the CSC setting.** Noise, Blur, Weather, and Digital are the main corruption groups in (Hendrycks and Dietterich 2019).

of corruption, underscoring its effectiveness in mitigating error accumulation and catastrophic forgetting. Further, in a rigorous 10-round CTTA experiment (in the Appendix) where the 15 corruption sequences were repeated, DPCore’s performance not only consistently exceeded SOTA but also showed improvement over time, illustrating its sustained robustness and adaptability in long-term adaptation scenarios.

In addition, the coreset’s growth in this setting is depicted in Fig. 3. DPCore strategically grouped the 15 types of corruption into distinct coreset elements based on their characteristics, although not strictly one per type as might be expected. For homogeneous groups like Noise (Gaussian, Shot, Impulse), DPCore efficiently condensed them into a single coreset, recognizing the similarities among these corruptions. This not only demonstrates DPCore’s ability to categorize and respond to similar target domains but also optimizes the number of coreset elements used. However, this approach varied with the complexity of the corruption types. For example, in the Digital group, which includes Contrast, Elastic, Pixel, and JPEG, multiple coreset elements were necessary. Particularly for Contrast, a more complex domain

Table 4: **mIoU score for Cityscapes-to-ACDC in the *Continual Structured Change (CSC)* setting.** The same target domains are repeated three times.

Algorithm	Round 1					Round 2					Round 3					Mean↑	Gain↑
	Fog	Night	Rain	Snow	Mean↑	Fog	Night	Rain	Snow	Mean↑	Fog	Night	Rain	Snow	Mean↑		
Source	69.1	40.3	59.7	57.8	56.7	69.1	40.3	59.7	57.8	56.7	69.1	40.3	59.7	57.8	56.7	56.7	0.0
TENT (Wang et al. 2021)	69.0	40.2	60.1	57.3	56.7	68.3	39.0	60.1	56.3	55.9	67.5	37.8	59.6	55.0	55.0	55.7	-1.0
CoTTA (Wang et al. 2022)	70.9	41.2	62.4	59.7	58.6	70.9	41.1	62.6	59.7	58.6	70.9	41.0	62.7	59.7	58.6	58.6	+1.9
DePT (Gao et al. 2022)	71.0	40.8	58.2	56.8	56.5	68.2	40.0	55.4	53.7	54.3	66.4	38.0	47.3	47.2	49.7	53.4	-3.3
VDP (Gan et al. 2023)	70.5	41.1	62.1	59.5	58.3	70.4	41.1	62.2	59.4	58.2	70.4	41.0	62.2	59.4	58.2	58.2	+1.5
SAR (Niu et al. 2023)	69.0	40.2	60.1	57.3	56.7	69.0	40.3	60.0	67.8	59.3	67.5	37.8	59.6	55.0	55.0	57.0	+0.3
EcoTTA (Song et al. 2023)	68.5	35.8	62.1	57.4	56.0	68.3	35.5	62.3	57.4	55.9	68.1	35.3	62.3	57.3	55.8	55.8	-0.9
ViDA (Liu et al. 2023b)	71.6	43.2	66.0	63.4	61.1	73.2	44.5	67.0	63.9	62.2	73.2	44.6	67.2	64.2	62.3	61.9	+5.2
DPCore (Proposed)	71.9	49.2	66.1	63.2	62.6	73.6	48.9	66.1	63.1	62.9	72.9	48.8	67.1	63.1	63.0	62.8	+6.1

Table 5: **Average mIoU score for Cityscapes-to-ACDC in the *Continual Dynamic Change (CDC)* setting.**

Algorithm	Fog	Night	Rain	Snow	Mean↑	Gain↑
Source	69.1	40.3	59.7	57.8	56.7	0.0
Tent	67.2	38.1	59.0	55.4	54.9	-1.8
CoTTA	69.5	40.9	61.2	57.4	57.3	+0.5
DePT	68.2	39.7	58.3	55.4	55.4	-1.3
VDP	70.2	40.1	61.0	58.2	57.4	+0.7
SAR	69.0	41.2	59.6	57.3	56.8	+0.1
EcoTTA	68.2	34.1	61.7	57.2	55.3	-1.4
ViDA	70.6	41.5	62.6	62.2	59.2	+2.5
DPCore	71.7	45.2	63.8	63.2	61.0	+4.3

where the source pre-trained model’s error was notably high at 91.4%, DPCore significantly improved performance by reducing the error to 50.4%, an improvement of **41.4%**. To achieve this, DPCore learned six distinct coreset elements for Contrast alone, underlining its advanced capability to adapt and effectively minimize the domain gap in more challenging scenarios. Overall, while DPCore managed to limit the total number of coreset elements to 15, the distribution across the corruption types was strategically varied based on the complexity and similarity of the domains involved, reflecting a sophisticated understanding of how to best manage and mitigate diverse target domains. This nuanced adaptation strategy ensures that DPCore not only conserves resources by minimizing unnecessary coreset creation but also maintains robustness by intensively focusing on where the domain challenge is greatest.

CIFAR10-to-CIFAR10C and CIFAR100-to-CIFAR100C. We further evaluated our method on CIFAR10-to-CIFAR10C and CIFAR100-to-CIFAR100C. As detailed at the top of Table 3, our approach not only consistently improves upon the performance of the source pre-trained model but also outperforms the previous SOTA. On CIFAR10C, DPCore achieves an impressive gain of **+9.8%** over the source model’s mean error rate, outperforming the next best result (ViDA) by **2.3%**. Similarly, for CIFAR100C, DPCore shows a gain of **+10.3%**, which is **2.2%** higher than the second-best performance by ViDA. Comprehensive results are available in the Appendix.

Cityscapes-to-ACDC. In addition to classification tasks, we also applied DPCore to the Cityscapes-to-ACDC dataset to validate its utility in real-world segmentation scenarios. In the CSC setting for segmentation, where the same sequence of target domains is repeated three times, we report the average mIoU scores for each cycle. As illustrated in Table 4,

DPCore consistently improves average mIoU scores across repetitions (62.6 \rightarrow 62.9 \rightarrow 63.0), demonstrating continual learning without performance degradation. Furthermore, our method surpasses the previous SOTA in each round, achieving a cumulative increase of 0.9% in mIoU while utilizing 99% fewer parameters than ViDA, as detailed in Table 8. These results underscore DPCore’s efficiency and effectiveness, marking it as a highly capable solution for semantic segmentation in structured domain scenarios.

Evaluation in the *CDC* Setting

Classification. We further evaluate the CTTA method in the proposed novel CDC setting. Results presented in Table 2 reveal that prior CTTA methods face significant challenges in this setting. The gains observed in the *CSC* setting diminish substantially in the more complex and realistic *CDC* setting, limiting their practical utility. For instance, the improvement by the previous SOTA, ViDA, dropped from +12.4% to +5.5%. In contrast, DPCore maintains a robust performance with only a slight decrease in improvement from +15.3% to +12.6%, still significantly outperforming the second best by **7.1%**. Additionally, while the number of coreset elements in the *CSC* setting was 15 in total, the dynamic nature of the *CDC* setting led DPCore to learn 25 coreset elements. This increase in coreset elements, with 10 additional compared to the *CSC* setting, reflects the method’s capacity to effectively group homogeneous domains even under challenging conditions. This consistent performance across both *CSC* and *CDC* settings highlights DPCore’s practical utility.

Segmentation. For the segmentation task, we applied the same strategy from the *CDC* setting to ACDC. The average IoU across three rounds is presented in Table 5, with comprehensive results available in the Appendix. Consistent with the classification task, prior CTTA methods exhibited degraded performance in this dynamic setting compared to the *CSC* setting. Notably, several methods such as Tent, DePT, and EcoTTA negatively impacted the performance of the source pre-trained model rather than enhancing it. The previous SOTA, ViDA, saw a reduction in improvement from +5.2% to +2.5% in this challenging environment. In contrast, our method adeptly managed the dynamic domain shifts, achieving a significant **+4.3%** improvement, compared to +6.1% in the *CSC* setting. Furthermore, our method consistently outperformed the compared methods across all four domains in this setting.

Analyses and Ablation Tests

We provide analyses and ablation studies for DPCore. All results are on ImageNet-to-ImageNet-C in the *CSC* setting.

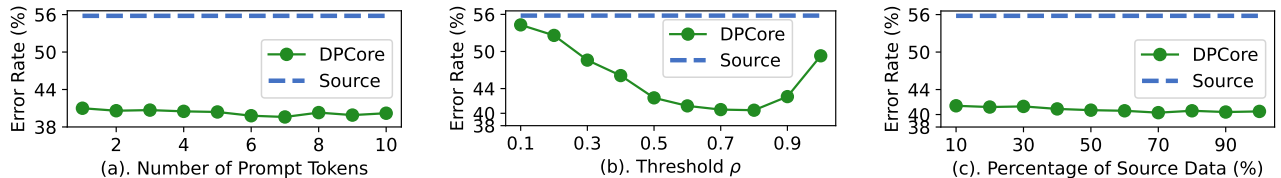


Figure 4: Ablation studies of DPCore. Experiments are conducted on ImageNet-to-ImageNet-C in the CSC setting.

Table 6: Ablation of each component in DPCore

	Source	$\rho = 0$	$\rho = 1$	$\rho = 0.8$
Dynamic Prompt Coreset	-	✓	-	✓
Weighted Updating Mechanism	-	-	✓	✓
Mean↓	55.8	54.8	49.3	40.5

Table 7: Effects of target batch size

	Source	BS= 8	BS= 16	BS= 32	BS= 50	BS= 64	BS= 100
Mean↓	55.8	46.2	45.8	41.1	40.4	40.5	40.1

More results are in the Appendix.

Number of Prompt Tokens l . We assess the impact of prompt size by varying the number of tokens, denoted as l , within the range of $\{1, 2, 3, \dots, 10\}$. As depicted in Fig. 4 (a), DPCore’s performance demonstrates only minor variations across different values of l , indicating a low sensitivity to the number of prompt tokens used. We standardize l at 4 for all main experiments. This decision aligns with typical testing conditions, where adjusting parameters based on test data is often impractical, thereby ensuring that our setup remains realistic and applicable in real-world scenarios.

Threshold ρ and Effectiveness of Each Component. The threshold ρ in Algo. 1 plays a crucial role in regulating the sensitivity of DPCore to domain changes. A lower ρ results in more batches being classified as OOD samples. For example, setting ρ to a value close to zero results in that each batch learns its own prompt (deviating from the *Weighted Updating Mechanism*). Conversely, a high ρ value means, aside from the initial batch, all subsequent batches are considered as ID samples, which reduces the coreset to just one element (bypassing the *Dynamic Prompt Coreset*). The results are illustrated in Fig. 4 (b). We have chosen $\rho = 0.8$ for all experiments to balance responsiveness with stability. The contributions of each component to the overall effectiveness of our system are detailed in Table 6.

Batch Size. We investigate the impact of batch size on DPCore’s performance in Table 7. The results indicate that performance remains quite stable for batch sizes of 32 and above. For batch sizes greater than 8 but smaller than 32, performance slightly declines but remains acceptable and is still comparable to that of ViDA, which is computed with a batch size of 50. A detailed discussion of batch sizes smaller

Table 8: Comparisons w.r.t. computation complexity

Algo.	#Param.	#FP	#BP	Relative time	Mean↓
Tent	0.03M	1	1	1.0	51.0
CoTTA	86.57M	3or35	1	3.6	54.8
VDP	1800	2	1	1.5	50.0
SAR	0.03M	1or2	0or2	2.0	45.6
EcoTTA	3.46M	1	1	1.9	48.0
ViDA	7.13M	2	1	2.8	43.4
Ours	0.04M	2	1	1.8	40.5

than 8 can be found in the Appendix.

Number of Source Data. To assess the impact of the volume of source data used to compute statistics on performance, we experimented with using varying proportions of the source dataset, specifically $\{10, 20, \dots, 100\}\%$. As illustrated in Fig. 4 (c), DPCore consistently enhances performance even with as little as 10% of the source data. For the purposes of this study, and to ensure a fair comparison, results are reported using the entire source dataset. This aligns with methodologies of other methods such as VDP, EcoTTA, and ViDA, which utilize the 100% source data to initialize or warm up their systems.

Efficiency Our method is computationally and memory efficiency. Beyond the requirements of the model itself, it necessitates only minimal additional resources for storing coreset and generating prompts, which is significantly less than the overall model size. In Table 8, we detail the number of learnable parameters (#Param.), the counts of forward and backward propagations (#FP/BP), and the relative computation time for processing a single batch in the CSC setting on ImageNet-to-ImageNet-C. We use the wall clock computation time of Tent as a baseline (indexed at 1.0) to compare the efficiency of other methods. Our method not only achieves substantial improvements over ViDA but does so with only 0.4% of the parameters used by ViDA and requires 35.7% less computation time. This efficiency demonstrates our approach’s capability to deliver enhanced performance while conservatively using computational resources.

Conclusion

We introduce DPCore, a robust and efficient framework for CTTA, distinguished by its innovative use of a *Dynamic Prompt Coreset* and *Weighted Updating Mechanism*. Our method not only demonstrates significant adaptability across dynamically changing environments but also ensures substantial computational and memory efficiency with minimal additional resource requirements beyond the core model. DPCore stands out by consistently outperforming SOTA CTTA methods, achieving remarkable improvements in both CSC and CDC settings. It also shows promising capabilities for broader applications in real-world scenarios where domain changes are unpredictable. To deepen the understanding of DPCore’s operational mechanics and its superior performance, we provide thorough analyses, including component-specific ablations and evaluations of various domain transition strategies. Additionally, visualizations of the coreset’s adaptations and their interactions with domain shifts are presented, offering intuitive insights into how DPCore effectively bridges the gap between source and target domains.

References

- Ben-David, S.; Blitzer, J.; Crammer, K.; and Pereira, F. 2006. Analysis of Representations for Domain Adaptation. In Schölkopf, B.; Platt, J.; and Hoffman, T., eds., *Advances in Neural Information Processing Systems*, volume 19. MIT Press.
- Boudiaf, M.; Mueller, R.; Ayed, I. B.; and Bertinetto, L. 2022. Parameter-free Online Test-time Adaptation. *2022 IEEE/CVF Conference on Computer Vision and Pattern Recognition (CVPR)*, 8334–8343.
- Cordts, M.; Omran, M.; Ramos, S.; Rehfeld, T.; Enzweiler, M.; Benenson, R.; Franke, U.; Roth, S.; and Schiele, B. 2016. The Cityscapes Dataset for Semantic Urban Scene Understanding. *2016 IEEE Conference on Computer Vision and Pattern Recognition (CVPR)*, 3213–3223.
- Dosovitskiy, A.; Beyer, L.; Kolesnikov, A.; Weissenborn, D.; Zhai, X.; Unterthiner, T.; Dehghani, M.; Minderer, M.; Heigold, G.; Gelly, S.; Uszkoreit, J.; and Houlsby, N. 2021. An Image is Worth 16x16 Words: Transformers for Image Recognition at Scale. In *International Conference on Learning Representations*.
- Duda, R. O.; and Hart, P. E. 1973. Pattern recognition and scene analysis.
- Gan, Y.; Bai, Y.; Lou, Y.; Ma, X.; Zhang, R.; Shi, N.; and Luo, L. 2023. Decorate the newcomers: Visual domain prompt for continual test time adaptation. In *Proceedings of the AAAI Conference on Artificial Intelligence*, volume 37, 7595–7603.
- Gao, Y.; Shi, X.; Zhu, Y.; Wang, H.; Tang, Z.; Zhou, X.; Li, M.; and Metaxas, D. N. 2022. Visual prompt tuning for test-time domain adaptation. *arXiv preprint arXiv:2210.04831*.
- Gao, Y.; Shi, X.; Zhu, Y.; Wang, H.; Tang, Z.; Zhou, X.; Li, M.; and Metaxas, D. N. 2023. Visual Prompt Tuning For Test-time Domain Adaptation.
- Ge, C.; Huang, R.; Xie, M.; Lai, Z.; Song, S.; Li, S.; and Huang, G. 2023. Domain adaptation via prompt learning. *IEEE Transactions on Neural Networks and Learning Systems*.
- Gong, T.; Jeong, J.; Kim, T.; Kim, Y.; Shin, J.; and Lee, S.-J. 2022. NOTE: Robust Continual Test-time Adaptation Against Temporal Correlation. In *Advances in Neural Information Processing Systems (NeurIPS)*.
- Hendrycks, D.; and Dietterich, T. 2019. Benchmarking neural network robustness to common corruptions and perturbations. *arXiv preprint arXiv:1903.12261*.
- Iwasawa, Y.; and Matsuo, Y. 2021. Test-Time Classifier Adjustment Module for Model-Agnostic Domain Generalization. In Ranzato, M.; Beygelzimer, A.; Dauphin, Y.; Liang, P.; and Vaughan, J. W., eds., *Advances in Neural Information Processing Systems*, volume 34, 2427–2440. Curran Associates, Inc.
- Jia, M.; Tang, L.; Chen, B.-C.; Cardie, C.; Belongie, S.; Hariharan, B.; and Lim, S.-N. 2022. Visual prompt tuning. In *European Conference on Computer Vision*, 709–727. Springer.
- Kingma, D. P.; and Ba, J. 2014. Adam: A method for stochastic optimization. *arXiv preprint arXiv:1412.6980*.
- Koh, P. W.; Sagawa, S.; Marklund, H.; Xie, S. M.; Zhang, M.; Balsubramani, A.; Hu, W.; Yasunaga, M.; Phillips, R. L.; Gao, I.; et al. 2021. Wilds: A benchmark of in-the-wild distribution shifts. In *International conference on machine learning*, 5637–5664. PMLR.
- Le, T.; Nguyen, T.; Ho, N.; Bui, H.; and Phung, D. 2021. LAMDA: Label Matching Deep Domain Adaptation. In Meila, M.; and Zhang, T., eds., *Proceedings of the 38th International Conference on Machine Learning*, volume 139 of *Proceedings of Machine Learning Research*, 6043–6054. PMLR.
- Lee, D.; Yoon, J.; and Hwang, S. J. 2024. BECoTTA: Input-dependent Online Blending of Experts for Continual Test-time Adaptation. In *International Conference on Machine Learning*.
- Lee, D.-H. 2013. Pseudo-Label : The Simple and Efficient Semi-Supervised Learning Method for Deep Neural Networks.
- Liang, J.; He, R.; and Tan, T. 2023. A Comprehensive Survey on Test-Time Adaptation under Distribution Shifts. *arXiv preprint arXiv:2303.15361*.
- Liang, J.; Hu, D.; and Feng, J. 2020. Do we really need to access the source data? source hypothesis transfer for unsupervised domain adaptation. In *International conference on machine learning*, 6028–6039. PMLR.
- Liu, C.; Wang, L.; Lyu, L.; Sun, C.; Wang, X.; and Zhu, Q. 2023a. Deja vu: Continual model generalization for unseen domains. *arXiv preprint arXiv:2301.10418*.
- Liu, J.; Yang, S.; Jia, P.; Lu, M.; Guo, Y.; Xue, W.; and Zhang, S. 2023b. ViDA: Homeostatic Visual Domain Adapter for Continual Test Time Adaptation. *arXiv preprint arXiv:2306.04344*.
- Liu, Z.; Lin, Y.; Cao, Y.; Hu, H.; Wei, Y.; Zhang, Z.; Lin, S.; and Guo, B. 2021. Swin transformer: Hierarchical vision transformer using shifted windows. In *Proceedings of the IEEE/CVF international conference on computer vision*, 10012–10022.
- Loshchilov, I.; and Hutter, F. 2017. Decoupled weight decay regularization. *arXiv preprint arXiv:1711.05101*.
- Mirza, M. J.; Micorek, J.; Possegger, H.; and Bischof, H. 2022. The norm must go on: Dynamic unsupervised domain adaptation by normalization. In *Proceedings of the IEEE/CVF conference on computer vision and pattern recognition*, 14765–14775.
- Mirza, M. J.; Soneira, P. J.; Lin, W.; Kozinski, M.; Possegger, H.; and Bischof, H. 2023. Actmad: Activation matching to align distributions for test-time-training. In *Proceedings of the IEEE/CVF Conference on Computer Vision and Pattern Recognition*, 24152–24161.
- Niloy, F. F.; Ahmed, S. M.; Raychaudhuri, D. S.; Oymak, S.; and Roy-Chowdhury, A. K. 2024. Effective restoration of source knowledge in continual test time adaptation. In *Proceedings of the IEEE/CVF Winter Conference on Applications of Computer Vision*, 2091–2100.

Niu, S.; Miao, C.; Chen, G.; Wu, P.; and Zhao, P. 2024. Test-Time Model Adaptation with Only Forward Passes. In *The International Conference on Machine Learning*.

Niu, S.; Wu, J.; Zhang, Y.; Chen, Y.; Zheng, S.; Zhao, P.; and Tan, M. 2022. Efficient test-time model adaptation without forgetting. In *International conference on machine learning*, 16888–16905. PMLR.

Niu, S.; Wu, J.; Zhang, Y.; Wen, Z.; Chen, Y.; Zhao, P.; and Tan, M. 2023. Towards stable test-time adaptation in dynamic wild world. *arXiv preprint arXiv:2302.12400*.

Recht, B.; Roelofs, R.; Schmidt, L.; and Shankar, V. 2019. Do imagenet classifiers generalize to imagenet? In *International conference on machine learning*, 5389–5400. PMLR.

Sakaridis, C.; Dai, D.; and Gool, L. V. 2021. ACDC: The Adverse Conditions Dataset with Correspondences for Semantic Driving Scene Understanding. *2021 IEEE/CVF International Conference on Computer Vision (ICCV)*, 10745–10755.

Schneider, S.; Rusak, E.; Eck, L.; Bringmann, O.; Brendel, W.; and Bethge, M. 2020. Improving robustness against common corruptions by covariate shift adaptation. *Advances in neural information processing systems*, 33: 11539–11551.

Shen, J.; Qu, Y.; Zhang, W.; and Yu, Y. 2018. Wasserstein distance guided representation learning for domain adaptation. In *Proceedings of the AAAI conference on artificial intelligence*, volume 32.

Song, J.; Lee, J.; Kweon, I. S.; and Choi, S. 2023. Ecotta: Memory-efficient continual test-time adaptation via self-distilled regularization. In *Proceedings of the IEEE/CVF Conference on Computer Vision and Pattern Recognition*, 11920–11929.

Sun, J.; Ibrahim, M.; Hall, M.; Evtimov, I.; Mao, Z. M.; Ferrer, C. C.; and Hazirbas, C. 2023. VPA: Fully Test-Time Visual Prompt Adaptation. In *Proceedings of the 31st ACM International Conference on Multimedia*, 5796–5806.

Sun, Y.; Wang, X.; Liu, Z.; Miller, J.; Efros, A.; and Hardt, M. 2020. Test-time training with self-supervision for generalization under distribution shifts. In *International conference on machine learning*, 9229–9248. PMLR.

Wang, D.; Shelhamer, E.; Liu, S.; Olshausen, B.; and Darrell, T. 2021. Tent: Fully Test-Time Adaptation by Entropy Minimization. In *International Conference on Learning Representations*.

Wang, Q.; Fink, O.; Van Gool, L.; and Dai, D. 2022. Continual test-time domain adaptation. In *Proceedings of the IEEE/CVF Conference on Computer Vision and Pattern Recognition*, 7201–7211.

Wightman, R. 2019. PyTorch Image Models. <https://github.com/rwightman/pytorch-image-models>.

Xie, E.; Wang, W.; Yu, Z.; Anandkumar, A.; Alvarez, J. M.; and Luo, P. 2021. SegFormer: Simple and Efficient Design for Semantic Segmentation with Transformers. In *Neural Information Processing Systems (NeurIPS)*.

Yuan, L.; Xie, B.; and Li, S. 2023. Robust test-time adaptation in dynamic scenarios. In *Proceedings of the IEEE/CVF Conference on Computer Vision and Pattern Recognition*, 15922–15932.

Appendix

Results for Baselines

In the conventional *CSC* setting, we reference results for all baseline methods from (Liu et al. 2023b) except for EcoTTA (Song et al. 2023) and SAR (Niu et al. 2023). For these, we employ the official implementations available at <https://github.com/Lily-Le/EcoTTA> and <https://github.com/mr-eggplant/SAR.git> to obtain the respective results. For the proposed *CDC* setting, we self-implement VDP (Gan et al. 2023) and DePT (Gao et al. 2022) while utilizing published codes to implement the other baseline methods.

Proofs of propositions

Suppose the batches B_0, \dots, B_t are naturally clustered into M mutually exclusive clusters G_1, G_2, \dots, G_M based on their distances. Abstractly, the algorithm \mathcal{A} outputs the current prompt $\mathbf{p}_t = \mathcal{A}(B_t, \dots, B_1)$ using the batch history B_1, \dots, B_t as input.

Algorithm 2: A simplified version of the proposed algorithm

```

1: for  $t = 1, 2, \dots, T$  do
2:   Compute the batch statistics  $\mathbf{s}(B_t)$  and distances
    $d_i = d(\mathbf{s}(B_t), \mathbf{s}^i)$ ,  $i = 1, \dots, N$ .
3:   if coreset is empty or  $\min_i d_i > \theta$  then
4:     Learn the prompt  $\mathbf{p}_t$  for  $B_t$  from scratch.
5:     Add a new core element  $(\mathbf{s}^{N+1}, \mathbf{p}_t)$  to the core-
   set.
6:      $N \leftarrow N + 1$ 
7:   else
8:     Assign  $B_t$  to the closest cluster  $j = \arg \min d_i$ .
9:     Learn the current prompt  $\mathbf{p}_t$  initialized with  $\mathbf{p}^j$ .
10:    Update  $j$ -th center:  $\mathbf{s}^j \leftarrow \mathbf{s}^j + \alpha(\mathbf{s}(B_t) - \mathbf{s}^j)$ .
11:    Update  $j$ -th prompt:  $\mathbf{p}^j \leftarrow \mathbf{p}^j + \alpha(\mathbf{p}_t - \mathbf{p}^j)$ .
12:   end if
13: end for

```

Let $\text{Conv}(G_i)$ be the convex hull of batches in G_i , $\text{diam}(S) = \sup_{x, x' \in S} d(x, x')$ be the diameter of a set S , $d(S, S') = \inf_{x \in S, x' \in S'} d(x, x')$ be the set distance, $\Pi^{(t-1)}$ be the set of permutations on $(1, \dots, t-1)$, $G_i(t)$ be the set of batches in i -th cluster at time t , and $\mathbf{s}^i(t)$ be the i -th core element (or center) at time t .

Assumption. We assume the clusters are *well-separated* defined as follows: there is $\theta > 0$ such that

$$\text{diam}(\text{Conv}(G_i)) < \theta < d(\text{Conv}(G_i), \text{Conv}(G_j)), \forall i \neq j.$$

Intuitively, this implies that points of the same group are closer to each other than points of different groups.

Proposition 1. For any $t \geq 1$, Alg. 2 assigns correct clusters to all the batches B_1, \dots, B_t .

Proof. We will prove by induction. At time 1, there are no existing batches so B_1 will be assigned to cluster 1 and $\mathbf{s}^1 = \mathbf{s}(B_1)$ at the end of the loop. Suppose the cluster assignments for batches B_1, \dots, B_{t-1} are correct. Since each center \mathbf{s}^i is updated by the interpolation of the previous

value $(1 - \alpha)\mathbf{s}^i$ and new value $\alpha\mathbf{s}(B_t)$, it is always inside the convex hull of batches belonging to the cluster, i.e., $\mathbf{s}^i(t) \in \text{Conv}(G_i(t))$.

When a new batch B_t that belongs to cluster j arrives at time t , either $|G_j(t-1)| = 0$ or $|G_j(t-1)| > 0$ (that is, there is either no or at least one batch from cluster j already.) When $|G_j(t-1)| = 0$, either $|G_k(t-1)| = 0, \forall k \neq j$ or $\exists k \neq j, |G_k(t-1)| > 0$, that is, there is either no batch or at least one batch from a different cluster. So there are four cases. If $|G_j(t-1)| = 0$ and $|G_k(t-1)| = 0, \forall k \neq j$, then B_t is the very first batch ($t = 1$) and will create a new cluster j . If $|G_j(t-1)| = 0$ and $\exists k \neq j, |G_k(t-1)| > 0$, we have $d(\mathbf{s}(B_t), \mathbf{s}^k) > \theta$ by well-separatedness and B_t will create a new cluster j . If $|G_j(t-1)| > 0$ and $|G_k(t-1)| = 0, \forall k \neq j$, we have $d(\mathbf{s}(B_t), \mathbf{s}^j) < \theta$ by well-separatedness and B_t will be correctly assigned to cluster j . If $|G_j(t-1)| > 0$ and $\exists k \neq j, |G_k(t-1)| > 0$, we have $d(\mathbf{s}(B_t), \mathbf{s}^j) < \theta < d(\mathbf{s}(B_t), \mathbf{s}^k)$ and B_t will be correctly assigned to cluster j . \square

Proposition 2. For any $t > 1$, Alg. 2 assigns B_t to the correct cluster independent of the batch order $B_{\pi(1)}, \dots, B_{\pi(t-1)}$, $\forall \pi \in \Pi^{(t-1)}$. Furthermore, if $\alpha = \frac{1}{|G_j|}$, then the center $\mathbf{s}^i(t)$ is the group mean $\mathbf{s}^i(t) = \frac{1}{|G_i(t)|} \sum_{B \in G_i(t)} B$, which is also independent of the order of B_1, \dots, B_t .

Proof. The inductive proof of Proposition 1 only requires the correctness in the previous time step to get correct assignment at the current time step and the order of batches has no impact on it under the well-separatedness assumption. Therefore B_{t-1} will also be correctly clustered for any $\pi \in \Pi^{(t-1)}$. Suppose $B^{(1)}, B^{(2)}, \dots$ are the batches assigned to cluster j in the order of assignment. Then from the update rule of Alg. 2 with $\alpha = \frac{1}{|G_j|}$, we get $\mathbf{s}^j = B^{(1)}$, $\mathbf{s}^j = \frac{1}{2}(B^{(1)} + B^{(2)})$, $\mathbf{s}^j = \frac{1}{3}(B^{(1)} + B^{(2)} + B^{(3)})$, etc. Since it's the mean of all batches, \mathbf{s}^j is also independent of the order π . \square

Proposition 3. For any $t > 1$, Alg. 2 returns the prompt \mathbf{p}_t for batch B_t independent of the batch order $B_{\pi(1)}, \dots, B_{\pi(t-1)}$, $\forall \pi \in \Pi^{(t-1)}$.

Proof. From Proposition 2, cluster assignment is independent of the order of B_1, \dots, B_{t-1} . At time t , there are two possibilities for the current batch B_t . If B_t belongs to one of the existing (say i -th) cluster. In that case, \mathbf{p}_t is learned starting from \mathbf{p}_i of the closest center. Since \mathbf{p}_i is independent of π , the learned \mathbf{p}_t is also independent of π . If, on the other hand, B_t does not belong to any existing clusters, then \mathbf{p}_t will be learned from scratch and therefore will also be independent of π . \square

Limitations.

While our method significantly advances test-time adaptation, its limitations may affect its wider application. Firstly, it requires access to source statistics, limiting its use where such data is unavailable. Secondly, it assumes each batch's

Table 9: Average error rate (%) of DPCore-DU across various batch size and K on ImageNet-to-ImageNet-C in *CSC* setting.

	Source	K= 8	K= 16	K= 32	K= 64
BS=1	55.8	48.2	47.9	47.4	46.8
BS=2	55.8	47.5	47.1	46.7	46.3
BS=4	55.8	47.1	46.4	45.9	45.5

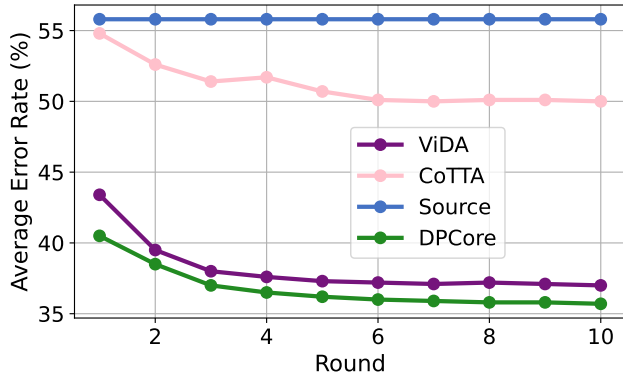


Figure 5: 10 rounds on ImageNet-to-ImageNet-C in *CSC* setting.

data comes from the same domain, which may not be the case in mixed-domain environments.

Comprehensive Results

In this section, we present the fine-grained results for Table 3 and Table 5. Table 10 and Table 11 show the full results for **CIFAR10-to-CIFAR10C** in *CSC* and *CDC* respectively. Table 12 and Table 11 display the full results for **CIFAR100-to-CIFAR100C** in *CSC* and *CDC* respectively. Table 5 shows the full results for **Cityscapes-to-ACDC** in *CDC* setting. The same batch order is used for all three rounds.

Additional Results

10 Rounds Experiment on ImageNet-to-ImageNet-C. In line with established practices (Wang et al. 2022; Liu et al. 2023b), we assess our method by repeating the ImageNet-to-ImageNet-C evaluation ten times in the *CSC* setting. As illustrated in Fig. 5, DPCore consistently outperforms both ViDA (Liu et al. 2023b) and CoTTA (Wang et al. 2022) throughout all ten rounds. Moreover, the average error rate progressively declines as the adaptation process continues, demonstrating DPCore’s robust ability to mitigate the issues of catastrophic forgetting and error accumulation often encountered in CTTA.

DPCore with Small Batch Size. In the main paper, we demonstrate that DPCore performs effectively when the batch size is eight or larger. However, challenges arise with smaller batch sizes, particularly when dealing with extremely small batches—such as a single data point per batch. To address this, we introduce a delayed update strategy, termed DPCore-DU, which adapts to continuous streams of

test data more effectively. Specifically, updates to DPCore are deferred until after accumulating a predefined number of samples, denoted as K . Prior to updating, we temporarily store the `CLS` feature of each batch. This approach is evaluated in the *Continual Structured Change (CSC)* setting with various values of K . As indicated in Table 9, DPCore-DU maintains performance comparable to other baselines, effectively handling the complications introduced by smaller batch sizes.

Discussion on Proposed *CDC* Setting. In this study, we introduce the *CDC* setting, a more realistic and challenging scenario for CTTA. While (Niu et al. 2023) proposes a wild TTA setting that considers mixed distribution shifts within each batch without changes across batches, our *CDC* setting focuses on dynamically changing environments where each batch may originate from different domains, and domain shifts occur at the batch level. Additionally, (Lee, Yoon, and Hwang 2024) introduces a scenario with continual gradual shifts, where the domain boundaries are blurred and domains may contain mixed data as they transition, yet still change in a structured manner similar to (Niu et al. 2023). Our approach, however, addresses domain changes in a more intricate manner, allowing for the reoccurrence of the same domain multiple times, with each occurrence varying in duration. This enhances the complexity and realism of the test-time adaptation challenges addressed by our model.

Furthermore, we rigorously test the *CDC* setting with varying distributions on ImageNet-to-ImageNet-C. We generate ten distinct random distributions encompassing all fifteen corruption types and their respective batch counts. We then apply our method to these varied settings. The average error rate for each of these distributions is documented in Table 15. The results demonstrate that our method is minimally impacted by these differing distributions, underscoring the robustness of DPCore in dynamically shifting domains.

Table 10: Classification error rate (%) for CIFAR10-to-CIFAR10C in the *Continual Structured Change (CSC)* setting.

Algorithm	Gauss.	Shot	Impulse	Defocus	Glass	Motion	Zoom	Snow	Frost	Fog	Bright	Contrast	Elastic	Pixel	JPEG	Mean↓	Gain↑
Source	60.1	53.2	38.3	19.9	35.5	22.6	18.6	12.1	12.7	22.8	5.3	49.7	23.6	24.7	23.1	28.2	0.0
Tent (Wang et al. 2021)	57.7	56.3	29.4	16.2	35.3	16.2	12.4	11.0	11.6	14.9	4.7	22.5	15.9	29.1	19.5	23.5	+4.7
CoTTA (Wang et al. 2022)	58.7	51.3	33.0	20.1	34.8	20	15.2	11.1	11.3	18.5	4.0	34.7	18.8	19.0	17.9	24.6	+3.6
VDP(Gan et al. 2023)	57.5	49.5	31.7	21.3	35.1	19.6	15.1	10.8	10.3	18.1	4	27.5	18.4	22.5	19.9	24.1	+4.1
ViDA (Liu et al. 2023b)	52.9	47.9	19.4	11.4	31.3	13.3	7.6	7.6	9.9	12.5	3.8	26.3	14.4	33.9	18.2	20.7	+7.5
DPCore(Proposed)	49.4	46.1	18.1	10.2	30.7	11.4	8.2	8.1	9.8	11.6	3.8	21.4	12.3	18.5	16.4	18.4	+9.8

Table 11: Classification error rate (%) for CIFAR10-to-CIFAR10C in the *Continual Dynamic Change (CDC)* setting.

Algorithm	Gauss.	Shot	Impulse	Defocus	Glass	Motion	Zoom	Snow	Frost	Fog	Bright	Contrast	Elastic	Pixel	JPEG	Mean↓	Gain↑
Source	60.1	53.2	38.3	19.9	35.5	22.6	18.6	12.1	12.7	22.8	5.3	49.7	23.6	24.7	23.1	28.2	0.0
Tent (Wang et al. 2021)	57.4	51.7	34.2	18.2	35.1	22.4	16.9	11.8	12.6	21.6	5.1	36.7	22.1	24.3	23.2	26.2	+2.0
CoTTA (Wang et al. 2022)	59.2	54.8	45.1	20.5	36.1	21.9	19.1	11.6	12.1	21.2	6.1	35.1	22.5	21.7	19.7	27.1	+1.1
VDP(Gan et al. 2023)	58.1	51.2	32.2	22.4	34.8	20.4	15.6	11.2	11.4	20.1	4.9	30.4	20.4	22.7	19.9	25.0	+3.2
ViDA (Liu et al. 2023b)	56.4	50.8	28.4	16.7	32.5	15.2	13.7	10.1	10.4	13.5	4.2	26.5	19.4	35.1	21.2	23.6	+4.6
DPCore(Proposed)	49.5	48.2	24.5	13.9	31.5	12.2	10.2	8.7	10.2	12.8	4.0	22.5	16.8	20.1	18.5	20.2	+8.0

Table 12: Classification error rate (%) for CIFAR100-to-CIFAR100C in the *Continual Structured Change (CSC)* setting.

Algorithm	Gauss.	Shot	Impulse	Defocus	Glass	Motion	Zoom	Snow	Frost	Fog	Bright	Contrast	Elastic	Pixel	JPEG	Mean↓	Gain↑
Source	55.0	51.5	26.9	24.0	60.5	29.0	21.4	21.1	25.0	35.2	11.8	34.8	43.2	56.0	35.9	35.4	0.0
Tent (Wang et al. 2021)	53.0	47.0	24.6	22.3	58.5	26.5	19.0	21.0	23.0	30.1	11.8	25.2	39.0	47.1	33.3	32.1	+3.3
CoTTA (Wang et al. 2022)	55.0	51.3	25.8	24.1	59.2	28.9	21.4	21.0	24.7	34.9	11.7	31.7	40.4	55.7	35.6	34.8	+0.6
VDP (Gan et al. 2023)	54.8	51.2	25.6	24.2	59.1	28.8	21.2	20.5	23.3	33.8	7.5	11.7	32.0	51.7	35.2	32.0	+3.4
ViDA (Liu et al. 2023b)	50.1	40.7	22.0	21.2	45.2	21.6	16.5	17.9	16.6	25.6	11.5	29.0	29.6	34.7	27.1	27.3	+8.1
DPCore (Proposed)	48.2	40.2	21.3	20.2	44.1	21.1	16.2	18.1	15.2	22.3	9.4	13.2	28.6	32.8	25.5	25.1	+10.3

Table 13: Classification error rate (%) for CIFAR100-to-CIFAR100C in the *Continual Dynamic Change (CDC)* setting.

Algorithm	Gauss.	Shot	Impulse	Defocus	Glass	Motion	Zoom	Snow	Frost	Fog	Bright	Contrast	Elastic	Pixel	JPEG	Mean↓	Gain↑
Source	55.0	51.5	26.9	24.0	60.5	29.0	21.4	21.1	25.0	35.2	11.8	34.8	43.2	56.0	35.9	35.4	0.0
Tent (Wang et al. 2021)	53.5	46.5	26.2	25.8	61.0	28.1	23.5	21.7	22.6	30.9	11.0	24.4	41.3	49.1	36.7	33.5	+1.9
CoTTA (Wang et al. 2022)	53.3	51.9	27.1	26.3	60.5	29.2	21.3	22.5	23.5	35.6	13.7	33.7	41.6	59.1	39.4	35.9	-0.5
VDP (Gan et al. 2023)	56.6	53.5	31.8	29.1	63.9	33.9	23.5	25.7	29.9	38.5	12.1	15.5	34.0	53.8	39.6	36.1	-0.7
ViDA (Liu et al. 2023b)	50.1	42.1	23.9	23.3	48.1	23.7	19.5	18.7	18.5	29.6	11.6	36.1	32.6	37.1	32.8	29.8	+5.6
DPCore (Proposed)	54.0	42.5	23.5	22.8	45.3	21.4	18.6	21.2	16.8	23.2	10.0	15.1	35.7	34.6	25.9	27.4	+8.0

Table 14: mIoU score for Cityscapes-to-ACDC in the *Continual Dynamic Change (CDC)* setting. The same target domains are repeated three times.

Algorithm	Round 1					Round 2					Round 3					Mean↑	Gain↑
	Fog	Night	Rain	Snow	Mean↑	Fog	Night	Rain	Snow	Mean↑	Fog	Night	Rain	Snow	Mean↑		
Source	69.1	40.3	59.7	57.8	56.7	69.1	40.3	59.7	57.8	56.7	69.1	40.3	59.7	57.8	56.7	56.7	0.0
Tent (Wang et al. 2021)	68.5	39.8	59.7	58.3	56.6	67.0	38.1	58.9	55.3	54.8	66.1	36.4	58.4	52.6	53.4	54.9	-1.8
CoTTA (Wang et al. 2022)	70.1	41.2	61.9	58.6	58.0	69.7	41.0	61.4	57.2	57.3	68.7	40.5	60.3	56.4	56.5	57.3	+0.5
DePT (Gan et al. 2023)	69.5	40.2	58.7	56.2	56.2	68.4	39.8	58.3	55.7	55.6	66.7	39.1	57.9	54.3	54.5	55.4	-1.3
VDP (Gan et al. 2023)	70.5	40.8	61.9	59.2	58.1	70.1	40.3	61.2	57.8	57.4	70.0	39.2	59.9	57.6	56.7	57.4	+0.7
SAR (Niu et al. 2023)	69.1	41.6	59.9	57.5	57.0	68.8	41.2	59.7	57.4	56.8	69.1	40.8	59.2	57.0	56.5	56.8	+0.1
EcoTTA (Song et al. 2023)	68.4	34.6	61.8	57.4	55.6	68.1	34.3	61.6	57.2	55.3	68.1	33.4	61.7	57.0	55.1	55.3	-1.4
ViDA (Liu et al. 2023b)	71.0	42.1	64.2	62.9	60.1	70.6	41.5	62.1	62.1	59.1	70.2	40.9	61.5	61.6	58.6	59.2	+2.5
DPCore (Proposed)	71.9	46.3	64.1	63.3	61.4	71.6	45.1	63.4	63.1	60.8	71.6	44.2	63.9	63.2	60.7	61.0	+4.3

Table 15: Average error rate (%) of DPCore across 10 different CSC settings on ImageNet-to-ImageNet-C. Uniform is used in the main paper experiments.

Source	Uniform	Random 1	Random 2	Random 3	Random 4	Random 5	Random 6	Random 7	Random 8	Random 9	Random 10	Average	
Mean↓	55.8	43.2	42.1	42.8	44.2	43.5	43.5	42.7	43.9	44.4	44.7	43.0	43.5